Hyperfine interactions of Ho^{3+} ions in KY_3F_{10}: Electron paramagnetic resonance and optical spectroscopy studies

D. S. Pytalev,* E. P. Chukalina, and M. N. Popova
Institute of Spectroscopy RAS, Moscow, Troitsk 142190, Russia

G. S. Shakurov
Zavoisky Physical-Technical Institute RAS, Kazan 420029, Russia

B. Z. Malkin and S. L. Korableva
Kazan Federal University, Kazan 420008, Russia

(Received 29 May 2012; revised manuscript received 3 August 2012; published 18 September 2012)

We use high-frequency electron paramagnetic resonance (EPR) and high-resolution optical Fourier spectroscopies to characterize hyperfine interactions of the impurity Ho^{3+} ions in KY_3F_{10} crystals. Well-resolved hyperfine structure is observed in the EPR spectra for several transitions within the ground $^5I_8$ multiplet of the Ho^{3+} ion and in the optical spectra for many lines in the infrared and visible ranges. The observed hyperfine patterns and field dependences of the resonance frequencies in the EPR spectra are well reproduced by calculations based on the crystal field (CF) theory. This favors reliability of calculated energies and wave functions of the electron-nuclear states within the ground and excited levels of Ho^{3+} in KY_3F_{10}. Finally, the dc magnetic susceptibility of the concentrated KHo_3F_{10} crystal taken from literature is successfully modeled in the temperature range 0.01–20 K, using CF parameters of the impurity Ho^{3+} ions in KY_3F_{10}.

DOI: 10.1103/PhysRevB.86.115124 PACS number(s): 71.70.−d, 71.55.Ht, 76.30.Kg, 78.20.Bh

I. INTRODUCTION

Revival of the interest in investigations of hyperfine interactions in the rare earth (R) ions is connected with a promising perspective to build an effective multilevel system on the basis of electron-nuclear (hyperfine) levels for applications in quantum information storage and optical manipulation. Because of long optical and hyperfine coherence times and a possibility to achieve a high-optical density, R-containing crystals are considered among the best candidates for development of quantum information systems at low temperatures (see, e.g. Refs. 1 and 2 and references therein). Knowledge of precise energies, symmetries, and wave functions of hyperfine sublevels of both the ground and optically excited states is crucial in order to create a well-defined multilevel system (in particular, with a Λ-type pattern of allowed optical transitions) to be used as an optical logical cell. To analyze the hyperfine structure (HFS) of the ground state, electron paramagnetic resonance (EPR) spectroscopy is a powerful tool.[3] As for the excited state, a spectral line broadening usually prevents one from resolving HFS in optical spectra. In these cases, some characteristics of HFS can be found from spectral hole burning experiments, while parameters of the hyperfine interaction are determined by calculations.[4,5] On rare occasions, an optically resolved HFS can be used to verify validity of these computations, and the search for crystals with resolved HFS in optical spectra remains a challenging task.

In a recent article,[6] some of us have reported on the well-resolved HFS of several lines in optical spectra of KY_3F_{10}:Ho^{3+}. The KY_3F_{10} crystal has a cubic structure (space group $Fm3m$).[7] The basic building unit consists of the two ionic groups $[KY_3F_8]^{2+}$ and $[KY_3F_{12}]^{2-}$, which alternate in the directions of the cubic axes (see Fig. 1). Trivalent R ions substitute for the Y^{3+} ions. Each R ion is surrounded by eight fluorine ions forming a square antiprism with the C_{4v} point symmetry group (see Fig. 1; the distances between an Y^{3+} ion and F^- ions at the corners of the two squares, normal to the C_4 symmetry axis and rotated by the angle of $\pi/4$ relative to one another, equal 0.2352 and 0.2202 nm).[8] There are three equivalent R centers oriented along three different C_4 axes of the cubic lattice structure. The compound is chemically and thermally stable, transparent, isotropic, and easy to grow. Once doped with R ions, it has received much attention since it is suitable to build solid-state lasers,[9,10] white-light emitters,[11,12] and quantum cutting systems to enhance solar cell efficiency.[13] Recently, KY_3F_{10} doped with Yb^{3+} ions was mentioned among the most promising hosts for laser cooling.[14]

Optical and EPR spectra of R ions in KY_3F_{10} crystals were broadly investigated. From laser excitation, fluorescence, and absorption spectra in the infrared and visible regions, crystal field (CF) energies of the ground and some excited multiplets were measured, and the CF analysis was carried out for Pr^{3+},[15] Nd^{3+},[16] Sm^{3+},[16,17] Eu^{3+},[18] Gd^{3+},[16] Dy^{3+},[16] Ho^{3+},[19] Er^{3+},[16,20,21] Tm^{3+},[22] and Yb^{3+}.[16] However, no HFS could be resolved in all these rather low-resolution optical studies. Note that the results of spectroscopic studies were of great importance for understanding the low-temperature magnetic ordering in concentrated KR_3F_{10} (R = Tb, Dy, Er, Tm, Yb) crystals containing sublattices with mutually orthogonal Ising-like magnetic moments coupled by dipole-dipole and exchange interactions.[23,24]

In this paper, we measure high-resolution (0.01 cm^{-1}) broadband optical spectra of KY_3F_{10}:Ho^{3+} and supplement the optical spectroscopy data with the high-frequency EPR study of several transitions within the ground $^5I_8$ multiplet of Ho^{3+} in KY_3F_{10} (the EPR spectra of this compound, earlier published by some of us,[25,26] have demonstrated HFS of only one transition, between the ground and the first excited singlet

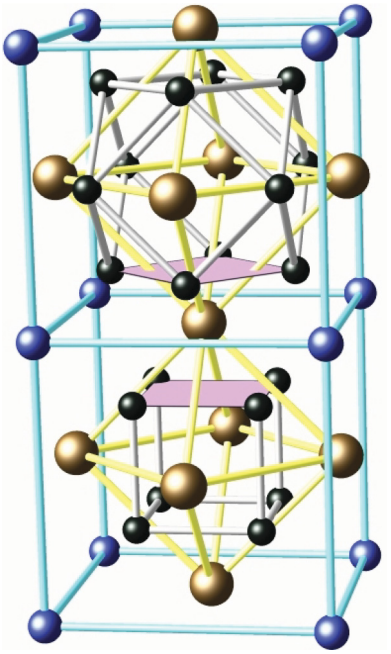

FIG. 1. (Color online) The unit cell of the $Fm3m$ structure of KY_3F_{10}. The large bronze (light gray) spheres substitute for yttrium atoms, the medium blue (gray) ones for potassium atoms, and the small black ones for fluorine atoms. The nearest surrounding of yttrium ions is represented by eight fluorine ions forming a square antiprism with the C_{4v} point symmetry group.

CF states). We simulate the observed hyperfine patterns in both optical and EPR spectra using energies and wave functions of the electron-nuclear states calculated in the framework of the CF theory. The CF parameters necessary for these calculations were obtained from the analysis of the measured high-resolution optical and EPR spectra. To additionally check the reliability of the derived CF parameters, we compare a calculated temperature dependence of the dc susceptibility of the concentrated isomorphic compound KHo_3F_{10} with experimental data available from literature.[27] Our research is an example of a combined approach, based on the magnetic resonance and optical measurements, to the study of hyperfine interactions in R-containing crystals.

II. EXPERIMENT

KY_3F_{10} single crystals doped with holmium (0.4 and 1 at.%) were grown by the Bridgman method, as described in Ref. 6.

High-resolution (up to 0.01 cm^{-1}) transmission spectra were measured in broad spectral (5000–23 000 cm^{-1}) and temperature (4–300 K) ranges using a Fourier spectrometer Bruker IFS 125HR and a closed-cycle cryostat Cryomech ST 403. The KY_3F_{10} crystals have a cubic structure and, therefore, absorb isotropically. So, it is in no sense taking polarized transmission spectra.

Electron paramagnetic resonance spectra were registered by making use of a tunable high-frequency EPR spectrometer based on a backward wave oscillator,[28] in the 175–650 GHz frequency range at the temperature 4.2 K in the magnetic field up to 0.95 T. The upper frequency limit of the spectrometer

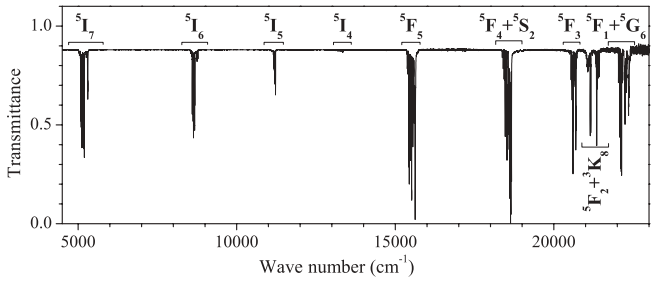

FIG. 2. Transmission spectrum of KY_3F_{10}:Ho^{3+} (1at.%) at 40 K.

was broadened up to 850 GHz using a generating unit of a dielectric terahertz spectrometer (produced by the Prokhorov General Physics Institute of Russian Academy of Sciences, Moscow, Russia).

III. EXPERIMENTAL RESULTS

A. Energies and symmetries of the Ho^{3+} CF levels in KY_3F_{10}

The Ho^{3+} ion imbedded into a crystal lattice has a rich spectrum in the near infrared and visible spectral ranges due to, mainly, forced electric dipole (ED) and magnetic dipole (MD) optical transitions between different states of the electronic $4f^{10}$ configuration (see Fig. 2). A particular $^{2S+1}L_J$ level of a free Ho^{3+} ion splits into $\Gamma_{1,2,3,4}$ singlets and Γ_5 doublets in the CF of KY_3F_{10} (Γ_k is the irreducible representation of the C_{4v} point symmetry group; see the first and second columns in Table I). The transitions involving Γ_5 levels are allowed both as ED and MD; other allowed ED transitions are $\Gamma_i \leftrightarrow \Gamma_i$ ($i = 1, \ldots, 4$) while the MD ones are $\Gamma_1 \leftrightarrow \Gamma_2$ and $\Gamma_3 \leftrightarrow \Gamma_4$. We interpret the observed spectra using these selection rules. The hot bands originating from the excited CF levels of the ground multiplet were discriminated by a temperature dependence of the intensity of spectral lines.

Figure 3 shows different optical multiplets observed in the transmission spectra at the temperatures of 5 and 20 K. Here, the spectral lines are labeled according to the following notations: the CF levels of the ground multiplet are numerated, and those of a given excited multiplet are marked by capital letters (A, B, etc.). We consider the $^5I_8 \rightarrow {}^5I_6$ optical transition [see Figs. 3(a) and 3(b)] in detail as an example of identification of CF levels. The $^5I_6$ multiplet splits into 10 sublevels, $2\Gamma_1 + \Gamma_2 + 2\Gamma_3 + 2\Gamma_4 + 3\Gamma_5$, in the CF of the C_{4v} point symmetry. At low temperature (5 K), excited sublevels of the lowest $^5I_8$ multiplet are depopulated, so that only transitions from the ground Γ_1 singlet and the first excited Γ_2 singlet can be observed in the spectrum. Thus, taking into account selection rules for optical transitions in the C_{4v} point symmetry group, one can obtain positions of the $2\Gamma_1 + \Gamma_2 + 3\Gamma_5$ energy levels. To determine the CF level symmetry, we took into account large widths of spectral lines involving transitions to the Γ_5 doublets, which are broadened as a rule by the hyperfine interaction and even have a resolved hyperfine structure in some cases. With temperature increasing, transitions from excited CF levels of the $^5I_8$ ground multiplet grow in intensity while the intensities of transitions from the two lowest singlets decrease. Lines corresponding to transitions from the Γ_5 excited doublets at 19.4 and 48 cm^{-1} are well observed at 20 K. As transitions from the Γ_5 doublets

TABLE I. Experimental E_{exp} and calculated E_{calc} CF energies and total hyperfine splittings Δ_{HFS} of the CF levels (all in cm^{-1}).

$^{2S+1}L_J$	Γ_i	E_{exp}	E_{calc}	Δ_{HFS}
$^5I_8$	$^1\Gamma_1$	0	0	0.0123
	$^1\Gamma_2$	5.8	5.8	0.0350
	$^1\Gamma_5$	19.4	19.5	0.9047
	$^2\Gamma_5$	48.0	48.9	0.5306
	$^1\Gamma_3$	94.8	92.5	0.0078
	$^1\Gamma_4$	110.0	111.7	0.0030
	$^2\Gamma_3$		126.7	0.0163
	$^2\Gamma_4$		167.3	0.0036
	$^3\Gamma_5$		208.5	0.1814
	$^2\Gamma_1$		233.4	0.0168
	$^4\Gamma_5$		247.2	1.3185
	$^2\Gamma_2$		280.1	0.6266
	$^3\Gamma_1$		280.1	0.6702
$^5I_7$	$^1\Gamma_2$	5115.8	5113	0.0052
	$^1\Gamma_1$	5120.7	5119	0.0466
	$^1\Gamma_5$	5127.0	5124	0.3475
	$^2\Gamma_5$	5136.5	5135	0.7743
	$^1\Gamma_4$	5139.9	5137	0.0200
	$^1\Gamma_3$	5178.0	5178	0.0092
	$^3\Gamma_5$	5193.7	5194	0.1840
	$^2\Gamma_2$	5202.5	5203	0.0350
	$^2\Gamma_4$	5207.1	5210	0.2297
	$^2\Gamma_3$	5210.0	5212	0.2553
	$^4\Gamma_5$	5304.8	5318	1.4419
$^5I_6$	$^1\Gamma_1$	8635.6	8627	0.0006
	$^1\Gamma_2$	8642.0	8634	0.0626
	$^1\Gamma_5$	8644.5	8636	0.3837
	$^1\Gamma_3$	8646.8	8637	0.1084
	$^2\Gamma_5$	8663.0	8660	0.7583
	$^2\Gamma_1$	8673.4	8671	0.0486
	$^1\Gamma_4$	8675.5	8674	0.0843
	$^3\Gamma_5$	8678.1	8675	0.3078
	$^2\Gamma_3$	8793.3	8806	0.5603
	$^2\Gamma_4$	8796.5	8806	0.6014
$^5I_5$	$^1\Gamma_5$	11 204	11 186	0.4806
	$^1\Gamma_4$	11 210.8	11 192	0.0320
	$^1\Gamma_2$	11 215.7	11 203	0.0147
	$^1\Gamma_1$	11 224.7	11 212	0.0228
	$^2\Gamma_5$	11 227.2	11 215	0.041
	$^1\Gamma_3$	11 233.1	11 223	0.0224
	$^2\Gamma_2$	11 235.7	11 225	0.0036
	$^3\Gamma_5$	11 334.0	11 337	1.3099
$^5I_4$	$^1\Gamma_3$		13 140	0.0007
	$^1\Gamma_4$		13 197	0.0040
	$^1\Gamma_5$	13 267.8	13 245	0.5746
	$^2\Gamma_5$	13 308.5	13 295	0.1272
	$^1\Gamma_1$	13 358.7	13 344	0.0078
	$^1\Gamma_2$		13 409	0.0476
	$^2\Gamma_1$		13 415	0.0888
$^5F_5$	$^1\Gamma_2$	15 437.0	15 428	0.0234
	$^1\Gamma_1$	15 440.5	15 432	0.0215
	$^1\Gamma_5$	15 473.1	15 461	0.4675
	$^1\Gamma_4$	15 532.7	15 518	0.0076
	$^2\Gamma_5$	15 534.7	15 550	0.7719
	$^1\Gamma_3$	15 573.0	15 577	0.0108
	$^3\Gamma_5$	15 626.0	15 626	0.1707
	$^2\Gamma_2$	15 649.0	15 650	0.0096
$^5F_4 + {}^5S_2$	$^1\Gamma_1$	18 450.9	18 449	0.0044
	$^1\Gamma_4$	18 452.8	18 453	0.0044
	$^1\Gamma_3$	18 468.0	18 470	0.0049
	$^1\Gamma_5$	18 483.9	18 483	0.0644
	$^1\Gamma_2$	18 520.8	18 512	0.0497
	$^2\Gamma_1$	18 521.5	18 515	0.0293
	$^2\Gamma_4$	18 621.0	18 608	0.0081
	$^2\Gamma_3$	18 624.0	18 613	0.0169
	$^2\Gamma_5$	18 630.3	18 617	0.0827
	$^3\Gamma_5$	18 638.9	18 627	0.2369
	$^3\Gamma_1$	18 665.1	18 648	0.0112
$^5F_3$	$^1\Gamma_5$	20 591.6	20 580	0.5403
	$^1\Gamma_2$	20 621.4	20 607	0.0112
	$^1\Gamma_3$	20 691.2	20 690	0.0422
	$^2\Gamma_5$	20 697.8	20 690	0.1675
	$^1\Gamma_4$	20 730.9	20 735	0.0008
$^5F_2 + {}^3K_8$	$^1\Gamma_4$		21 082	0.0039
	$^1\Gamma_1$		21 090	0.0086
	$^1\Gamma_3$		21 124	0.0045
	$^1\Gamma_5$	21 165.3	21 171	0.1832
	$^2\Gamma_1$		21 334	0.7291
	$^1\Gamma_2$		21 334	0.7328
	$^2\Gamma_5$	21 350.7	21 350	1.4473
	$^3\Gamma_1$	21 362.7	21 349	0.0525
	$^2\Gamma_4$	21 369.8	21 373	0.0125
	$^3\Gamma_5$	21 373.3	21 359	0.1334
	$^2\Gamma_3$		21 391	0.0076
	$^3\Gamma_4$	21 400.2	21 400	0.0068
	$^3\Gamma_3$	21 406.0	21 406	0.0537
	$^4\Gamma_5$	21 422.6	21 417	0.5943
	$^5\Gamma_5$	21 428.0	21 432	1.0953
	$^2\Gamma_2$	21 435.1	21 433	0.1536
	$^4\Gamma_1$	21 436.5	21 435	0.0275
$^5F_1 + {}^5G_6$	$^1\Gamma_4$	22 084.0	22 075	0.2115
	$^1\Gamma_3$	22 085.5	22 076	0.2270
	$^1\Gamma_1$	22 122.6	22 106	0.0204
	$^1\Gamma_5$	22 135.7	22 116	0.1317
	$^2\Gamma_4$	22 145.7	22 140	0.0008
	$^2\Gamma_3$		22 206	0.0065
	$^2\Gamma_5$		22 244	0.4665
	$^1\Gamma_2$		22 312	0.0136
	$^3\Gamma_5$	22 314.0	22 314	0.8343
	$^2\Gamma_1$		22 321	0.0177
	$^4\Gamma_5$		22 328	0.5392
	$^2\Gamma_2$		22 409	0.0175

are allowed to all CF levels, positions of the Γ_3 and Γ_4 singlets can be obtained. However, in the case of high-frequency lines, $3I$, $3J$, $4I$, and $4J$, we had to use temperature dependence of their intensity to differentiate ambiguous transitions from the CF levels at 19.4 and 48 cm^{-1}. Normalized integral intensities of these transitions together with populations of the CF levels at 19.4 and 48.0 cm^{-1} given by Boltzmann distribution are plotted in Fig. 3(b) (inset). Thus, we succeeded in getting information on all CF levels of the $^5I_6$ multiplet. The spectral lines $1D$ (8646.8 cm^{-1}) and $1G$ (8675.5 cm^{-1}) in Fig. 3(a) corresponding to the forbidden transitions $^5I_8(^1\Gamma_1) \rightarrow {}^5I_6(^1\Gamma_3)$ and $^5I_8(^1\Gamma_1) \rightarrow {}^5I_6(^1\Gamma_4)$, respectively, borrow their intensity

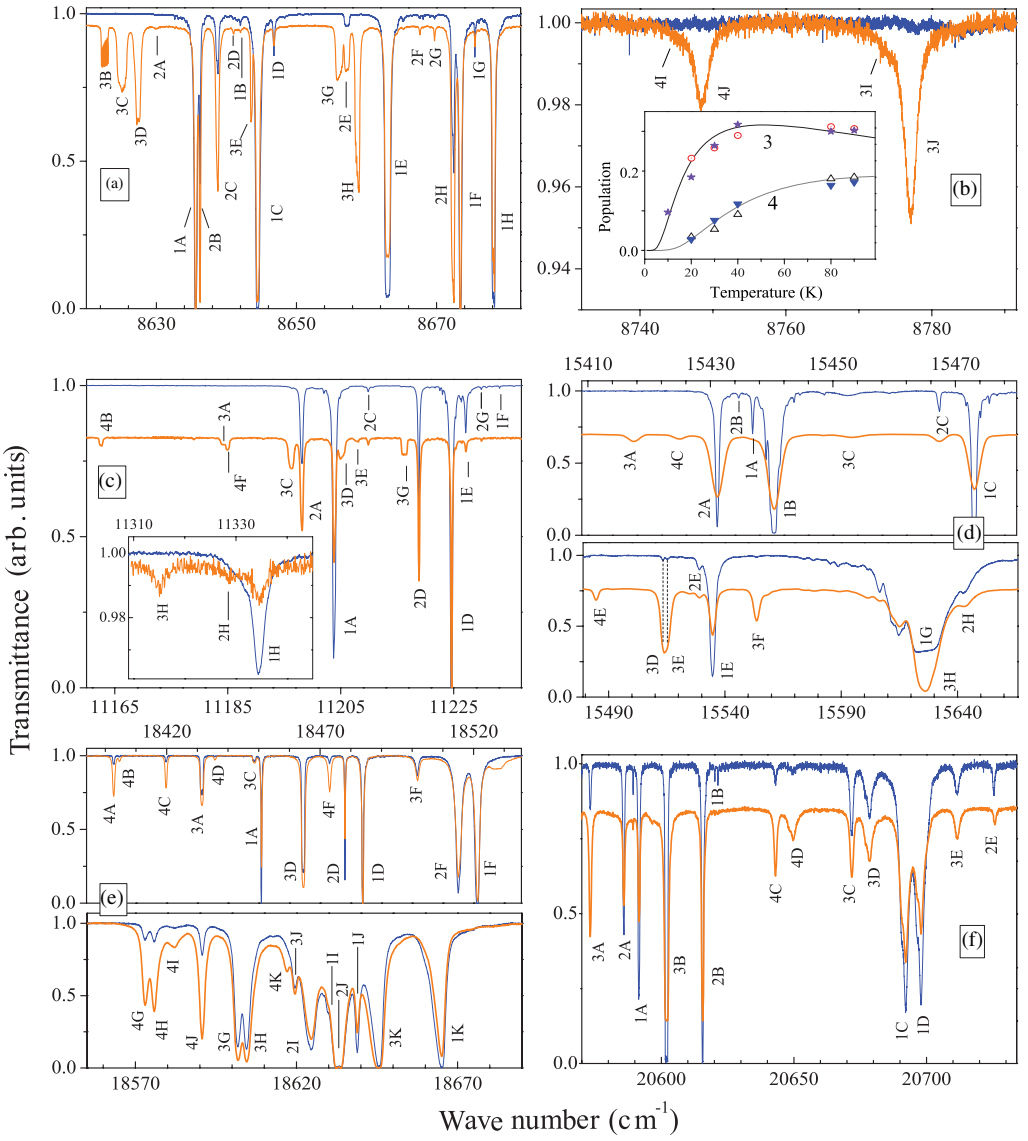

FIG. 3. (Color online) Transmission spectra in the range of the (a) and (b) $^5I_6$, (c) $^5I_5$, (d) $^5F_5$, (e) $^5F_4 + {}^5S_2$, and (f) $^5F_3$ multiplets in KY_3F_{10}:Ho^{3+} at the temperatures of 5 K [blue (black) traces] and 20 K [orange (gray) traces]. The inset in (b) compares the Boltzmann distribution of populations of the excited levels 3 (at 19.4 cm^{-1}) and 4 (at 48.0 cm^{-1}) (solid curves) and the normalized experimental integral intensities of the spectral lines: $3I$ (open circles), $3J$ (solid stars), $4I$ (open triangles), and $4J$ (solid triangles). The inset in (c) is given for the high-frequency part of the $^5I_5$ multiplet.

from allowed $\Gamma_1 \leftrightarrow \Gamma_5$ transitions due to mixing of the $^1\Gamma_3$ and $^1\Gamma_4$ singlets in the $^5I_6$ multiplet with the closely spaced $^1\Gamma_5$ and $^3\Gamma_5$ doublets, respectively, by the magnetic hyperfine interaction.

Energy level positions of the next two multiplets, $^5I_5$ and $^5I_4$, were not published before. It is worth noting that such information is significant since these levels play an important role in energy transfer processes in Ho^{3+}-doped compounds (see, e.g. Refs. 29 and 30). In this paper, we obtained positions of all CF levels of the $^5I_5$ multiplet, while due to weak absorption corresponding to the $^5I_8 \rightarrow {}^5I_4$ transition, the spectra reveal only three of seven CF levels of the $^5I_4$ multiplet. The data on the rest of the $^5I_4$ sublevels were derived from the theoretical analysis (see Sec. IV). The spectral line $1F$ corresponding to the forbidden transition $^5I_8(^1\Gamma_1) \rightarrow {}^5I_5(^1\Gamma_3)$ at 11 233 cm^{-1} was observed due to mixing of the $^1\Gamma_3$ and $^2\Gamma_5$ sublevels in the $^5I_5$ multiplet by the hyperfine interaction.

In the visible part of the spectrum, the $^5S_2$, $^3K_8$, and $^5G_6$ optical multiplets overlap with the $^5F_4$, $^5F_2$, and $^5F_1$ multiplets, respectively, which makes the analysis more complicated. Based on the experimental spectra, we were able to get positions of all energy levels of the $^5F_{5,4,3}$ and $^5S_2$ multiplets [Figs. 3(d)–3(f)]. Unfortunately, many lines corresponding to the transitions $^5I_8 \rightarrow {}^5F_{1,2}$, $^3K_8$, and $^5G_6$ were too weak to be resolved, and as a result positions of only 17 CF levels of these excited multiplets were determined. Table I summarizes our experimental data, part of which complement and correct those previously published in Ref. 19.

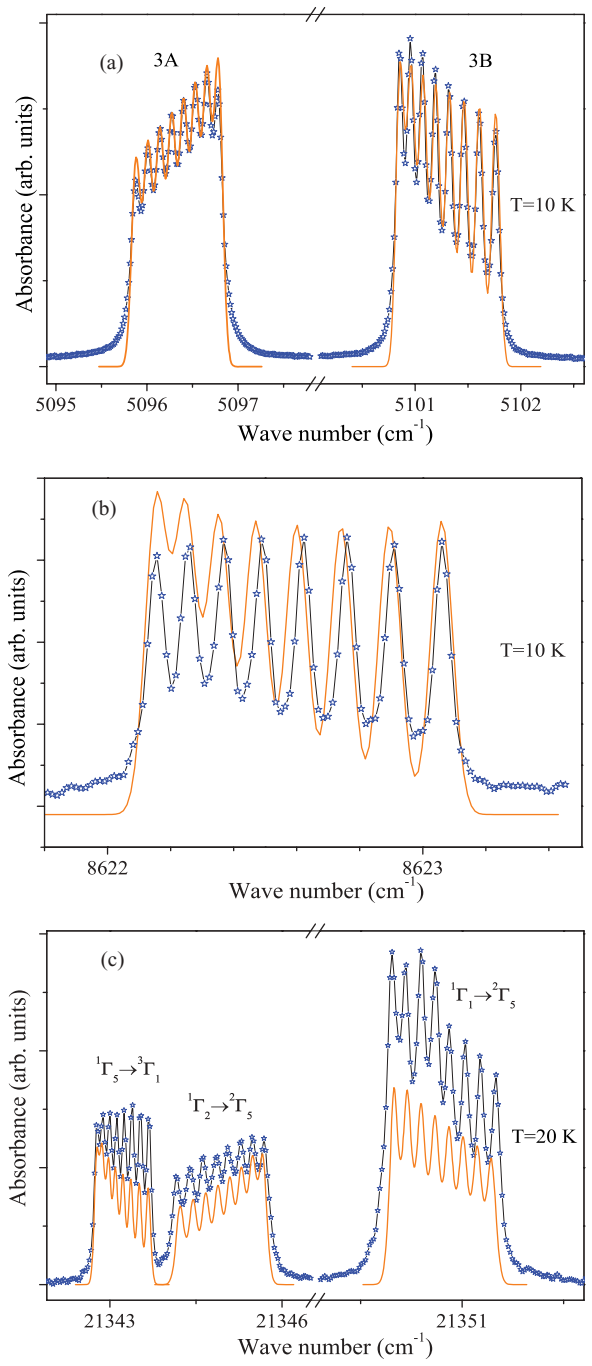

FIG. 4. (Color online) Measured [blue (black) line plus symbols] and simulated [orange (gray) curves] spectral lines corresponding to the doublet-singlet or singlet-doublet transitions in the transmission spectrum: (a) $^1\Gamma_5(^5I_8) \rightarrow {}^1\Gamma_2(^5I_7)$ $(3A)$ and $^1\Gamma_5(^5I_8) \rightarrow {}^1\Gamma_1(^5I_7)$ $(3B)$, (b) $^1\Gamma_5(^5I_8) \rightarrow {}^1\Gamma_2(^5I_6)$, (c) in the region of the $^3K_8$ optical multiplet.

B. Hyperfine patterns in optical and EPR spectra of Ho^{3+}:KY_3F_{10}

Well-resolved structure of optical transitions that involve the Γ_5 doublets was observed, caused by the hyperfine interaction between the $4f$ electrons and the nucleus of the only ^{165}Ho isotope having a nuclear spin $I = 7/2$. Some examples of hyperfine patterns are shown in Fig. 4. Most of the spectral lines with resolved HFS correspond to transitions from the

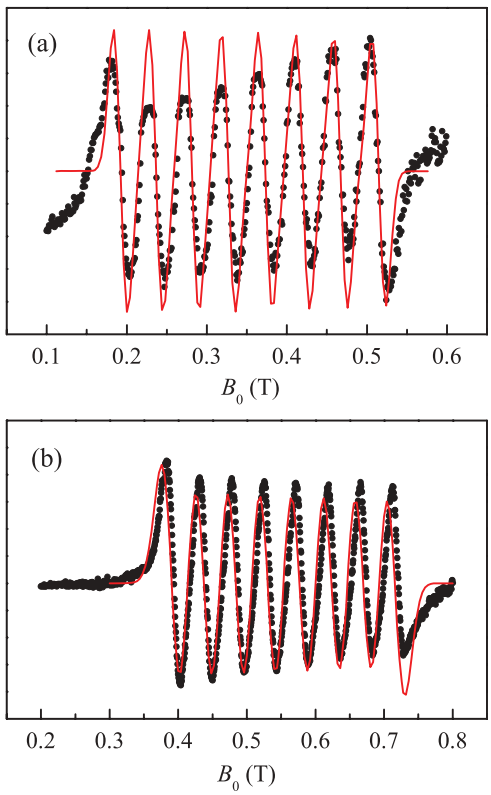

FIG. 5. (Color online) Recorded EPR signals in KY_3F_{10}:Ho^{3+} (black dots) and derivatives of the simulated absorption (red solid curves) (a) at the frequency 614 GHz in the magnetic fields $\boldsymbol{B}_0 \| C_4$, $\boldsymbol{B}_1 \perp \boldsymbol{B}_0$ and (b) at the frequency 189.5 GHz in the magnetic fields $\boldsymbol{B}_0 \| C_4$, $\boldsymbol{B}_1 \| \boldsymbol{B}_0$, $T = 4.2$ K.

$^1\Gamma_5(^5I_8)$ doublet, but several lines reflect the hyperfine splitting of the $^1\Gamma_5(^3K_8)$ doublet as well [see, e.g. Fig. 4(c)]. The halfwidth of the hyperfine components in the low-frequency part of optical multiplets is as small as 0.05 cm^{-1}, whereas the high-frequency lines are strongly broadened by nonradiative transitions to lower CF sublevels of the upper multiplet with creation of lattice phonons. The electric quadrupole hyperfine interaction and the nondiagonal part of the magnetic dipole (pseudoquadrupole) hyperfine interaction result in a slight nonequidistance of the observed HFS. To take an example, the first two hyperfine components of the $^1\Gamma_5(^5I_8) \rightarrow {}^1\Gamma_1(^5I_7)$ transition [Fig. 4(a), line $3B$] are spaced by 0.10 cm^{-1} while the last two are spaced by 0.16 cm^{-1}.

As we already mentioned in Sec. I, the EPR measurements described in Refs. 25 and 26 revealed the HFS of the $^1\Gamma_1(^5I_8) \rightarrow {}^1\Gamma_2(^5I_8)$ magnetic dipole transition between the ground and the first excited singlets. In this paper, we additionally studied transitions between these singlets and the first excited doublet which was involved in a majority of transitions that demonstrated well-resolved HFS in optical spectra.

Electron paramagnetic resonance spectra taken in an external constant magnetic field $\boldsymbol{B}_0$ parallel to the C_4 symmetry axis and a microwave field $\boldsymbol{B}_1$ normal to $\boldsymbol{B}_0$ at frequencies in the range 350–650 GHz as well as for $\boldsymbol{B}_1$ parallel to $\boldsymbol{B}_0$ at frequencies in the range 175–205 GHz contain resonance signals with well-resolved HFS. For this orientation of $\boldsymbol{B}_0$, only one type of magnetically nonequivalent C_{4v} centers

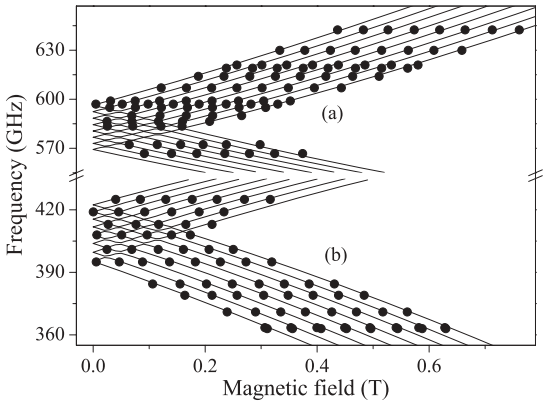

FIG. 6. Resonance frequencies of the (a) $^1\Gamma_1(^5I_8)$ singlet $\rightarrow$ $^1\Gamma_5(^5I_8)$ doublet and (b) $^1\Gamma_2(^5I_8)$ singlet $\rightarrow$ $^1\Gamma_5(^5I_8)$ doublet transitions in the EPR spectra of a KY_3F_{10}:Ho^{3+} single crystal in the magnetic fields $\boldsymbol{B}_0$ parallel to the C_4 axis (dots = experiment, solid curves = results of simulations).

with their symmetry axis collinear with $\boldsymbol{B}_0$ contributes into the EPR signals. Examples of the observed EPR signals are shown in Fig. 5. Figure 6 shows the field dependences of resonance frequencies corresponding to transitions between the $^1\Gamma_5(^5I_8)$ doublet and two singlets $^1\Gamma_1(^5I_8)$ and $^1\Gamma_2(^5I_8)$. Using these data, we measured the energy gaps between the CF singlets and the excited doublet. The obtained values of $E(^1\Gamma_5) - E(^1\Gamma_1) = 582 \pm 1$ GHz (19.4 ± 0.03 cm^{-1}) and $E(^1\Gamma_5) - E(^1\Gamma_2) = 409.7 \pm 1$ GHz (13.66 ± 0.03 cm^{-1}) are in good agreement with the optical measurements. In Fig. 6, each group of eight branches of resonance frequencies increasing (decreasing) with increasing magnetic field corresponds to transitions between the hyperfine sublevels of the singlets and of the upper (lower) Zeeman sublevel of the electronic doublet. The g factors ($g_\parallel = 12 \pm 0.5$, $g_\perp = 0$) of the $^1\Gamma_5(^5I_8)$ doublet were estimated from the angular dependence of the EPR lines corresponding to the $^1\Gamma_1(^5I_8) \rightarrow {}^1\Gamma_5(^5I_8)$ transition in the magnetic field $\boldsymbol{B}_0$ rotating in the (110) plane (not shown) when all three types of magnetically nonequivalent centers with mutually perpendicular tetragonal symmetry axes were observed.

IV. THEORETICAL CONSIDERATION

A. Simulation of hyperfine patterns in optical and EPR spectra of Ho^{3+}:KY_3F_{10}

To analyze the results of measurements, we consider the following Hamiltonian of the $^{165}Ho^{3+}$ ion in the C_{4v} symmetry CF of KY_3F_{10} operating in the space of 8008 electron-nuclear states of the ground electronic $4f^{10}$ configuration:

$$H = H_{\rm FI} + H_{\rm CF} + H_{\rm HF} + H_{\rm Q} + H_{\rm Z} + H_{\rm ZI}. \qquad (1)$$

The first term in Eq. (1), $H_{\rm FI}$, is the free-ion Hamiltonian defined by Slater parameters F^2, F^4, F^6 of the electrostatic interaction between the $4f$ electrons, the spin-orbit coupling constant ξ, two-particle parameters α, β, γ and three-particle parameters T^2, T^3, T^4, T^6, T^7, T^8 of the electrostatic configuration interaction, parameters P^2, P^4, P^6 and M^0, M^2, M^4 of correlated spin-orbit and spin-spin interactions, respectively.[31] The CF Hamiltonian $H_{\rm CF}$ can be defined in the local Cartesian system of coordinates (with the z axis along the C_4 symmetry axis of a particular impurity Ho^{3+} ion) by five CF parameters B_q^p:

$$H_{\rm CF} = \sum_k \left[B_0^2 C_{0,k}^{(2)} + B_0^4 C_{0,k}^{(4)} + B_0^6 C_{0,k}^{(6)} + B_4^4\left(C_{-4,k}^{(4)} + C_{4,k}^{(4)}\right) + B_4^6\left(C_{-4,k}^{(6)} + C_{4,k}^{(6)}\right)\right]. \qquad (2)$$

In Eq. (2), the sum is taken over ten $4f$ electrons with the radius-vectors $\boldsymbol{r}_k$, $C_{q,k}^{(p)} = C_q^{(p)}(\boldsymbol{r}_k/r_k)$ are the electronic spherical tensor operators. The term $H_{\rm HF}$ in Eq. (1) corresponds to the magnetic dipole hyperfine interaction:

$$H_{\rm HF} = 2\mu_B\gamma_{\rm Ho}\hbar\left\langle\frac{1}{r^3}\right\rangle_{4f}\sum_k\left\{\boldsymbol{I}\boldsymbol{l}_k + \frac{\sqrt{6}}{2}\left[\frac{2}{\sqrt{6}}C_{0,k}^{(2)}(3s_{kz}I_z - \boldsymbol{s}_k\boldsymbol{I}) + \left(C_{2,k}^{(2)} + C_{-2,k}^{(2)}\right)(s_{kx}I_x - s_{ky}I_y) - i\left(C_{2,k}^{(2)} - C_{-2,k}^{(2)}\right) \times (s_{kx}I_y + s_{ky}I_x) - \left(C_{1,k}^{(2)} - C_{-1,k}^{(2)}\right)(s_{kx}I_z + s_{kz}I_x) + i\left(C_{1,k}^{(2)} + C_{-1,k}^{(2)}\right)(s_{kz}I_y + s_{ky}I_z)\right]\right\}. \qquad (3)$$

Here, μ_B is the Bohr magneton, $\gamma_{\rm Ho}/2\pi = 8.98$ MHz/T is the gyromagnetic ratio for ^{165}Ho,[32] $\boldsymbol{l}_{\rm k}$ and $\boldsymbol{s}_{\rm k}$ are the orbital and spin moments, respectively, of $4f$ electrons, and $\boldsymbol{I}$ is the nuclear spin moment. The average value of r^{-3} for $4f$ electrons, $\langle r^{-3}\rangle_{4f} = 9.7$ at. units, was taken from Ref. 33. The next term in Eq. (1), $H_{\rm Q}$, corresponds to the electric quadrupole hyperfine interaction:

$$H_Q = \frac{e^2Q(1-\gamma_\infty)}{4I(2I-1)}\sum_L q_L\frac{3z_L^2 - r_L^2}{r_L^5}I_0 - \frac{\sqrt{6}e^2Q(1-R_Q)}{4I(2I-1)} \times\left\langle\frac{1}{r^3}\right\rangle_{4f}\sum_k\left[\frac{\sqrt{6}}{3}C_{0,k}^{(2)}I_0 + \left(C_{2,k}^{(2)} + C_{-2,k}^{(2)}\right)I_2 - i\left(C_{2,k}^{(2)} - C_{-2,k}^{(2)}\right)I_{-2} - \left(C_{1,k}^{(2)} - C_{-1,k}^{(2)}\right)I_1 + i\left(C_{1.k}^{(2)} + C_{-1.k}^{(2)}\right)I_{-1}\right]. \qquad (4)$$

Here, e is the proton charge, $I_0 = 3I_z^2 - I(I+1)$, $I_2 = I_x^2 - I_y^2$, $I_{-2} = I_xI_y + I_yI_x$, $I_1 = I_xI_z + I_zI_x$, $I_{-1} = I_zI_y + I_yI_z$, $\gamma_\infty = -80$ and $R_Q = 0.1$ are Sternheimer antishielding and shielding factors,[34] respectively, $Q = 2.394 \times 10^{-28}$ m^2 is the quadrupole moment of the ^{165}Ho nucleus.[32] The first term in Eq. (4) is proportional to the crystal lattice contribution into the electric field gradient at the nucleus and contains a sum over host lattice ions with charges eq_L and radius-vectors $\boldsymbol{r}_L$ relative to the considered holmium nucleus. This sum was computed by the Ewald method using the nominal ion charges $q(K^+) = 1$, $q(Y^{3+}) = 3$, $q(F^-) = -1$ and the lattice structure constants from Ref. 7, $\sum_L q_L(3z_L^2 - r_L^2)/r_L^5 = 61.1$ nm^{-3}. The last two terms in Eq. (1) correspond to the electronic and nuclear Zeeman energies in an external magnetic field $\boldsymbol{B}_0$: $H_{\rm Z} = -\boldsymbol{\mu}\boldsymbol{B}_0$, where $\boldsymbol{\mu} = -\mu_B\sum_k(\boldsymbol{l} + 2\boldsymbol{s})$ is the electronic magnetic moment of the Ho^{3+} ion, and $H_{\rm ZI} = -\gamma_{\rm Ho}\hbar\boldsymbol{I}\boldsymbol{B}_0$.

The CF energies $E_{\rm calc}$ (see Table I) and the corresponding electronic wave functions were obtained by numerical diagonalization of the Hamiltonian $H_0 = H_{\rm FI} + H_{\rm CF}$ in the space

TABLE II. CF parameters B_q^p (cm^{-1}).

p	q	Ref. 26	Ref. 19	This paper[a]
2	0	−568	−669	−647
4	0	−1332	−1269	−1309
4	4	406	344	359.2
6	0	576	525	470.8
6	4	−40	9	−5

[a]The total set of parameters involves the following free-ion parameters (in cm^{-1}): $F^2 = 94063$, $F^4 = 66681$, $F^6 = 51777$, $\xi = 2142$, $\alpha = 17.15$, $\beta = -608$, $\gamma = 1800$, $T^2 = 400$, $T^3 = 37$, $T^4 = 105$, $T^6 = -264$, $T^7 = 316$, $T^8 = 336$, $P^2 = 605$, $P^4 = 385$, $P^6 = 182$, $M^0 = 2.54$, $M^2 = 1.42$, $M^4 = 0.79$.

of 1001 Slater determinants constructed from single-electron wave functions of the $4f^{10}$ configuration. At the next step, the matrix of the Hamiltonian given by Eq. (1) computed in the truncated space of 146 × 8 = 1168 electron-nuclear states corresponding to lower 146 electronic CF states with energies below 24 100 cm^{-1} was numerically diagonalized. The obtained energies E_j of electron-nuclear states and the corresponding wave functions were used to simulate EPR signals and spectral envelopes in the optical spectra in zero magnetic field.

Calculations were carried out with parameters of the free-ion Hamiltonian presented in Ref. 19 except the Slater parameters $F^4 = 66\,681$ (66 361) cm^{-1} and $F^6 = 51\,777$ (51 637) cm^{-1} (values in brackets are from Ref. 19), which were determined, as well as the CF parameters given in Table II, from the fitting procedure to get the best agreement between the simulated and measured spectra. The CF parameters used in this paper are close to those obtained in Ref. 19 but considerably differ from parameters which have been found earlier in Refs. 25 and 26 from the analysis of the CF energy levels of the ground multiplet only (see Table II).

As is seen in Table I, the measured CF energies are satisfactorily reproduced by calculations (a root-mean-square deviation for 79 energy levels equals 9.3 cm^{-1}). In zero external magnetic field, CF singlets (doublets) give rise to four (eight) electron-nuclear doublets. The calculated total hyperfine splittings Δ_{HFS} (differences between energies of the upper and the lower hyperfine doublets generated by a particular CF energy level) are presented in Table I. The hyperfine splittings of CF singlets are of the second order in the magnetic hyperfine interaction and as a rule are much smaller than intervals between the hyperfine sublevels of the Γ_5 doublets. However, in the case of closely spaced singlets Γ_1 and Γ_2 or Γ_3 and Γ_4 ($^2\Gamma_2$ and $^3\Gamma_1$ in the $^5I_8$ multiplet, $^2\Gamma_4$ and $^2\Gamma_3$ in $^5I_7$, $^2\Gamma_3$ and $^2\Gamma_4$ in $^5I_6$, $^2\Gamma_1$ and $^1\Gamma_2$ in $^5F_2 + {}^3K_8$, see Table I) mixed by the hyperfine interaction, the calculated values of Δ_{HFS} are comparable to the hyperfine splittings of the Γ_5 doublets. The energies of the hyperfine sublevels of the ground $^1\Gamma_1$ state are 0, 184.9, 308.5, and 370.5 MHz.

The reliability of the set of CF parameters for the Ho^{3+} ions in KY_3F_{10} obtained in this paper was checked by the analysis of intervals between the individual spectral components and their relative intensities in the observed HFS of the EPR signals and the optical transitions. Spectral envelopes at a given temperature T were simulated according to the expression

$$I(\Gamma \to \Gamma', E) = \sum_{j\in\Gamma}\sum_{k\in\Gamma'}\sum_{\alpha=x,y,z} |\langle j|\mu_\alpha|k\rangle|^2 \exp\left[-E_j/k_BT - (E_k - E_j - E)^2/2\Delta^2_{\Gamma\Gamma'}\right], \quad (5)$$

where k_B is the Boltzmann constant, and the Gaussian line shape for all magnetic dipole transitions between the hyperfine sublevels of the initial (Γ) and final (Γ') CF states is assumed. Note that, though integral intensities of the MD transitions between sublevels of the multiplets with total angular moments differing by more than unity are much less than intensities of the ED ones, Eq. (5) is still valid when considering relative intensities of hyperfine structure components in the case of spectral lines corresponding to singlet-doublet transitions. The calculated hyperfine patterns are shown in Figs. 4 and 5, multiplied by a factor chosen to facilitate a comparison with the experimental data. To fit the observed HFS, the following halfwidths (in units of cm^{-1}) of individual hyperfine optical lines were used in calculations: $(2\ln 2)^{1/2}\Delta_{\Gamma\Gamma'} = 0.0566$ [$^5I_8(^1\Gamma_5) \to {}^5I_7(^1\Gamma_2)$], 0.0458 [$^5I_8(^1\Gamma_5) \to {}^5I_7(^1\Gamma_1)$], 0.0416 [$^5I_8(^1\Gamma_5) \to {}^5I_6(^1\Gamma_2)$], 0.0541 [$^5I_8(^1\Gamma_5) \to {}^3K_8(^3\Gamma_1)$], 0.090 [$^5I_8(^1\Gamma_1) \to {}^3K_8(^2\Gamma_5)$], and 0.090 [$^5I_8(^1\Gamma_2) \to {}^3K_8(^2\Gamma_5)$]. Envelopes of the microwave absorption spectra were simulated using slightly smaller values of the halfwidths, namely, $(2\ln 2)^{1/2}\Delta_{\Gamma\Gamma'} = 0.0307$ [$^5I_8(^1\Gamma_1) \to {}^5I_8(^1\Gamma_2)$] and 0.0336 [$^5I_8(^1\Gamma_1) \to {}^5I_8(^1\Gamma_5)$] ($cm^{-1}$). The results of the simulations reproduce well the experimental spectra including the intensity distributions. The calculated g factor of the $^1\Gamma_5(^5I_8)$ doublet $g_\parallel = 12.05$ coincides with the measured one, and the simulated field dependences of the resonance frequencies in the EPR spectra taken in the crossed constant and microwave fields also reproduce well the experimental data (see Fig. 6).

B. Modeling of the dc magnetic susceptibility of KHo_3F_{10}

Because ionic radii of the Ho^{3+} and Y^{3+} ions are almost the same,[35] we have good reason to believe that the obtained set of the CF parameters can be used to analyze magnetic properties of the concentrated crystal KHo_3F_{10}, which is isomorphic with KY_3F_{10}. Taking into account magnetic dipole-dipole interactions between the Ho^{3+} ions and using expressions for the local magnetic fields in KHo_3F_{10} derived in Ref. 36 in the framework of the mean-field approximation, we obtain the following expression for the isotropic dc magnetic susceptibility:

$$\chi = [\chi_\parallel + 2\chi_\perp - (2A + B - 4C)\chi_\parallel\chi_\perp]/3D. \quad (6)$$

Here, $\chi_\parallel$ and $\chi_\perp$ are the single-ion susceptibilities in magnetic fields parallel and perpendicular to the C_4 symmetry axis at the holmium site, respectively, and $D = (1 - A\chi_\parallel)(1 - B\chi_\perp) - 2C^2\chi_\parallel\chi_\perp$, $A = Q_{zz}(1,1) + Q_{zz}(1,2) - 2N$, $B = Q_{xx}(1,1) + Q_{zz}(1,2) + 2Q_{xx}(1,3) - 4N$, $C = 2(Q_{zz}(1,3) - N)$ [N is the demagnetizing factor and $Q_{\alpha\beta}(j,k)$ are the dipole lattice sums computed in Ref. 36]. For a spherical sample, we obtain $A = 0.03$, $B = -4.1628$, $C = 2.0964$ in units of $(4\pi/3v)$, where v is the unit cell volume. Figure 7 shows that a specific shape of the measured temperature dependence of the static magnetic susceptibility (in Ref. 27) with the well-pronounced contribution from the holmium nuclear magnetic moments enhanced by the hyperfine interaction in the Van

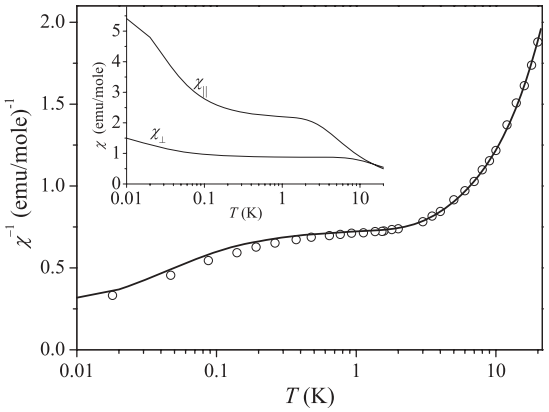

FIG. 7. Measured in Ref. 27 (symbols) and calculated (solid curve) inverse susceptibility of KHo_3F_{10} (spherical sample). Inset: computed single-ion susceptibilities in magnetic fields parallel ($\chi_{||}$) and perpendicular ($\chi_{\perp}$) to the symmetry axis of the local CF affecting the Ho^{3+} ion.

Vleck paramagnet KHo_3F_{10} at temperatures below 0.1 K is reproduced rather precisely by Eq. (6) when making use of the single-ion susceptibilities computed with the CF parameters of the impurity Ho^{3+} ions in KY_3F_{10} (see inset of Fig. 7).

V. CONCLUSION

High-resolution broadband optical transmission and high-frequency EPR spectra of the KY_3F_{10}:Ho^{3+} single crystals were studied, with the aim to characterize hyperfine interactions of Ho^{3+} ions in KY_3F_{10}. The observed hyperfine patterns in both optical and EPR spectra and field dependences of the resonance frequencies in the EPR spectra were successfully modeled using calculations based on the CF theory and taking into consideration magnetic dipole and electric quadrupole terms in the Hamiltonian of the hyperfine interaction. Explicit values for energies of the hyperfine sublevels of the ground state are given. All the peculiarities of the observed HFS are explained, including nonregular intervals and nonuniform intensity distribution between the hyperfine components of optical spectral lines. This consideration has evidenced a significant influence on the spectral shapes of the mixing between wave functions of different CF levels by the hyperfine interaction, which leads to strong nuclear spin projection mixing and relaxes the optical selection rules. The CF parameters necessary for these calculations were obtained from the fitting procedure to get the best agreement between the simulated and measured EPR and high-resolution optical spectra. The information on CF levels and CF parameters for the Ho^{3+} ions in KY_3F_{10} presented earlier in Ref. 19 on the basis of low-resolution (0.25 cm^{-1}) optical spectra was corrected and complemented, which is useful for laser applications. Finally, the experimental[27] dc magnetic susceptibility of the concentrated KHo_3F_{10} crystal was successfully modeled in the temperature range 0.01–20 K, by taking into account the magnetic dipole-dipole interactions between holmium ions and making use of the CF parameters of the dilute KY_3F_{10}:Ho paramagnet derived in this paper.

ACKNOWLEDGMENTS

This work was partly supported by the Russian Academy of Sciences under the Programs for Basic Research and by the Federal Program "Research and Education Personnel of Innovative Russia". D.P. also acknowledges a support from the Russian Foundation for Basic Research (Grant No. 12-02-31284).

*Corresponding author: pytalev@isan.troitsk.ru

[1]B. Lauritzen, N. Timoney, N. Gisin, M. Afzelius, H. de Riedmatten, Y. Sun, R. M. Macfarlane, and R. L. Cone, Phys. Rev. B **85**, 115111 (2012).
[2]M. P. Hedges, J. J. Longdell, Y. Li, and M. J. Sellars, Nature (London) **465**, 1052 (2010).
[3]O. Guillot-Noël, Ph. Goldner, Y. Le Du, E. Baldit, P. Monnier, and K. Bencheikh, Phys. Rev. B **74**, 214409 (2006).
[4]O. Guillot-Noël, Ph. Goldner, Y. Le Du, P. Loiseau, B. Julsgaard, L. Rippe, and S. Kröll, Phys. Rev. B **75**, 205110 (2007).
[5]O. Guillot-Noël, Ph. Goldner, E. Antic-Fidancev, and J. L. Le Gouët, Phys. Rev. B **71**, 174409 (2005); Ph. Goldner and O. Guillot-Noël, Mol. Phys. **102**, 1185 (2004).
[6]E. P. Chukalina, D. S. Pytalev, and M. N. Popova, Phys. Lett. A **375**, 3205 (2011).
[7]J. W. Pierce and Y. P. Hong, in *Proceedings of the Tenth Rare Earth Research Conference, Springfield, 1973*, edited by C. J. Kevane and T. Moeller (National Technical Information Service, Springfield, 1973), p. 529.
[8]K. Friese, H. Krüger, V. Kahlenberg, T. Balić-Zunić, H. Emerich, J. Y. Gesland, and A. Grzechnik, J. Phys.: Condens. Matter **18**, 2677 (2006).
[9]P. Camy, J. L. Doualan, R. Moncorgé, J. Bengoechea, and U. Weichmann, Opt. Lett. **32**, 1462 (2007).
[10]Y. Dong, S. T. Li, and X. H. Zhang, Laser Phys. Lett. **9**, 116 (2012).
[11]A. Toncelli, L. Bonelli, R. Faoro, D. Parisi, and M. Tonelli, Opt. Mater. **31**, 1205 (2009).
[12]T. Pang, W. Cao, M. Xing, X. Luo, and X. Yang, Opt. Mater. **33**, 485 (2011).
[13]D. Serrano, A. Braud, J.-L. Doualan, P. Camy, A. Benayad, V. Ménard, and R. Moncorgé, Opt. Mater. **33**, 1028 (2011).
[14]M. P. Hehlen, Proc. SPIE **7614**, 761404 (2010).
[15]J. P. R. Wells, M. Yamaga, T. P. J. Han, and H. G. Gallagher, J. Phys.: Condens. Matter **12**, 5297 (2000).
[16]R. Yu. Abdulsabirov, A. V. Vinokurov, V. A. Ivanshin, I. N. Kurkin, E. A. Pudovik, A. L. Stolov, and Sh. I. Yagudin, Opt. Spektrosk. **63**, 97 (1987) [Opt. Spektrosc. (USSR) **63**, 55 (1987)].
[17]J. P. R. Wells, A. Sugiyama, T. P. J. Han, and H. G. Gallagher, J. Lumin. **85**, 91 (1999).
[18]P. Porcher and P. Caro, J. Chem. Phys. **65**, 89 (1976).
[19]M. Mujaji and J. P. R. Wells, J. Phys.: Condens. Matter **21**, 255402 (2009).
[20]E. Boulma, M. Diaf, J. P. Jouart, M. Bouffard, J. L. Doualan, and R. Moncorgé, J. Phys.: Condens. Matter **18**, 6721 (2006).

[21] K. Heyde, K. Binnemans, and C. Görller-Warland, J. Chem. Soc. Faraday Trans. **94**, 1671 (1998).
[22] M. Diaf, A. Braud, C. Labbé, J. L. Doualan, S. Girard, J. Margerie, R. Moncorgé, and M. Thuau, Can. J. Phys. **77**, 693 (2000).
[23] S. L. Chamberlain, Gang Luo, and L. R. Corruccini, Phys. Rev. B **67**, 134414 (2003).
[24] S. L. Chamberlain and L. R. Corruccini, Phys. Rev. B **71**, 024434 (2005).
[25] B. Z. Malkin, V. F. Tarasov, and G. S. Shakurov, Pis'ma v Zh. Exp. Teor. Fiz. **62**, 789 (1995) [JETP Lett. **62**, 811 (1995)].
[26] V. F. Tarasov, G. S. Shakurov, B. Z. Malkin, and C. A. Hutchicon, Jr., J. Alloys Compd. **250**, 364 (1997).
[27] S. L. Chamberlain and L. R. Corruccini, J. Phys. Chem. Solids **67**, 710 (2006).
[28] V. F. Tarasov and G. S. Shakurov, Appl. Magn. Res. **2**, 571 (1991).
[29] T. H. Lee and J. Heo, Phys. Rev. B **73**, 144201 (2006).
[30] A. F. H. Librantz, S. D. Jackson, L. Gomes, S. J. L. Ribeiro, and Y. Messaddeq, J. Appl. Phys. **103**, 023105 (2008).
[31] H. M. Crosswhite and H. Crosswhite, J. Opt. Soc. Am. B **1**, 246 (1984).
[32] M. A. H. McCausland and I. S. Mackenzie, Adv. Phys. **28**, 305 (1979).
[33] A. Abragam and B. Bleaney, *Electron Paramagnetic Resonance of Transition Ions* (Oxford Univ. Press, Oxford, 1970).
[34] R. P. Gupta and S. K. Sen, Phys. Rev. A **7**, 850 (1973).
[35] R. D. Shannon, Acta Cryst. A **32**, 751 (1976).
[36] A. V. Vinokurov, B. Z. Malkin, and A. L. Stolov, Fiz. Tverd. Tela (S. Petersburg) **38**, 751 (1996) [Phys. Solid State **38**, 415 (1996)].